RPE | Radiation Physics & Engineering
A Peer-Reviewed Journal
Published by K.N. Toosi University of Technology
http://rpe.kntu.ac.ir
Research Article

Radiation Physics and Engineering 2025; 6(1):21–29

Determination of photon and electron fluence spectral variation for 6 MV medical linear accelerators by Monte Carlo simulation

Vida Khodabandeh Baygi, Laleh Rafat Motavalli*, Elie Hoseinian Azghadi

Physics Department, Faculty of Science, Ferdowsi University of Mashhad, Mashhad, Iran

HIGHLIGHTS

- The energy distribution and mean energy of the beams depend on spatial positions.
- The electron behavior is depth-dependent beyond the field edge.
- The Linear Energy Transfer electrons should be taken into account, as they affect healthy tissues around the tumor.
- Varian Clinac ix^{TM} tends to produce lower energy electrons than Elekta Precise^{TM} and Varian TrueBeam^{TM}.

ABSTRACT

During external beam radiation therapy, patients are exposed to secondary radiation sources, contributing to out-of-field doses with potential long-term adverse effects. Understanding photon and electron energy spectra is essential to evaluate the secondary effects of modern radiotherapy. This study aimed to evaluate the photon and electron fluence spectra and mean energy beyond the field edge as well as in-field regions for several small radiotherapy fields. The study used International Atomic Energy Agency (IAEA) phase-space files for the 6 MV photon beams produced by three commonly used linear accelerators to generate small and standard fields. The mean photon and electron energies were calculated at multiple depths and off-axis distances for the three linear accelerators and a predefined 6 MV spectrum. The study found that the photon fluence spectra strongly depend on spatial positions and vary significantly as a function of depth, off-axis distance, field size, and linac model. Furthermore, the behavior of electrons is depth-dependent beyond the field edge, where the mean electron energy near the surface is greater than in-field regions, especially in small fields, leading to surface dose enhancement.

KEYWORDS

BEAMnrc
FLURZnrc
Monte Carlo simulation
Mean energy

HISTORY

Received: 3 July 2024
Revised: 3 September 2024
Accepted: 17 September 2024
Published: Winter 2025

1 Introduction

Recent technological advancements have significantly improved the efficacy of radiation therapy in cancer treatment, leading to prolonged patient survival (Kry et al., 2017; Harrison, 2013; Sánchez-Nieto et al., 2020; Howell et al., 2006; Newhauser and Durante, 2011). However, during external beam radiotherapy, regardless of the target volume, patients are inevitably subjected to doses outside of the primary field due to secondary radiation sources, including treatment head leakage, collimator scattering, and patient scattering (Kry et al., 2006, 2017; Huang et al., 2013; Kase et al., 1983). Intensity-modulated radiation therapy (IMRT) exacerbates this issue by increasing out-of-field doses compared to conventional therapy as a result of a higher number of monitor units (MUs) and longer beam-on-time (Kry et al., 2005, 2006; Jang et al., 2007; Konefał et al., 2010). This is a significant drawback, as these out-of-field doses can manifest late secondary cancers and cardiac toxicity even at relatively small doses (Kry et al., 2017; Huang et al., 2013; Skrobala et al., 2017). Diallo et al. (Diallo et al., 2009) discovered that the majority of second cancers emerge in the margin of the irradiated target or the beam bordering region. Furthermore, healthy tissues near a tumor may be affected differently by radiation depending on low-energy radiations (electrons and photons) commonly present outside of the field edge (Xicohténcatl-Hernández et al., 2021). Thus, despite improved conformality, the problem of doses to normal tissues outside the treated volume has yet to be mitigated. To determine the risks of secondary cancers due to out-of-field doses, it is important to first understand the characteristics of the peripheral low-absorbed

*Corresponding author: rafat@um.ac.ir

https://doi.org/10.22034/rpe.2024.465869.1200

doses received by healthy organs surrounding the tumor (Skrobala et al., 2017; D'agostino et al., 2013).

Today, the methods employed in determining the radiation dose from external beam radiotherapy include measurements, treatment planning systems (TPSs), and Monte Carlo simulations (Newhauser et al., 2016). Treatment planning systems, however, failed to accurately compute doses beyond a few centimeters outside the treatment field (Sánchez-Nieto et al., 2020; Huang et al., 2013; Jang et al., 2008; Howell et al., 2010; Wang and Ding, 2014; Kruszyna et al., 2017). Conversely, measurements pose challenges as the radiation energy spectrum, dose rate, and overall dose distribution characteristics differ considerably outside the treatment field and require special consideration (Kry et al., 2017). The dosimeters commonly used in clinics to assess absorbed doses are energy-dependent, causing a significant challenge for accurate measurements (Xicohténcatl-Hernández et al., 2021). Since these dosimeters are calibrated within the beam central axis, they can provide misleading dose measurements outside the field due to their energy dependency (Kry et al., 2017; Skrobala et al., 2017; Xicohténcatl-Hernández et al., 2021; Edwards and Mountford, 2004; Bordy et al., 2013; Scarboro et al., 2011). Therefore, to calibrate dosimeters properly, a necessary step before measuring out-of-field doses is to determine the type of photon energy spectrum in the out-of-field region. Thus, there is a need for an improved method to determine the out-of-field spectrum from radiotherapy treatments. One prospective approach is the Monte Carlo method, which is known as a gold standard for radiation transport calculations (Chetty et al., 2007; Kry et al., 2006; Reynaert et al., 2005; Mesbahi et al., 2005).

It is important to have precise knowledge of beam characteristics, such as the mean photon and electron energy in small radiotherapy fields. This knowledge would allow for a better assessment of the biological effects on healthy organs and the development of appropriate correction factors for energy-dependent dosimeters.

Numerous studies have documented photon and electron energy spectra for various field sizes (Kry et al., 2006; Jang et al., 2007; Skrobala et al., 2017; Edwards and Mountford, 2004; Scarboro et al., 2011). Edwards and Mountford (Edwards and Mountford, 2004) studied the photon energy spectrum near a phantom surface outside the field edge and the corresponding spectrum on the central axis. They evaluated the potential impact of spectral differences on photon dosimetry by considering the sensitivity of two energy-dependent dosimeters outside the field edge in relation to the beam central axis. Scarboro et al. (Scarboro et al., 2011) evaluated the variability in the energy spectrum of a 6 MV photon beam for several field sizes of 5, 10, and 20 cm^2 at different depths and distances from the central axis. Their findings revealed an over-response of up to 12% outside the field edge compared to the central axis, with significant implications for the TLD energy-dependent dosimeter. Skrobala et al. (Skrobala et al., 2017) evaluated the photon mean energy for several depths and off-axis distances for a 10 cm^2 field size. The findings revealed a notable decrease in mean energies beyond the 6 MV photon beam at all depths. Jang et al. (Jang et al., 2007) found significant variations in photon and electron energy spectra in 3DCRT and IMRT photon fields, affecting the response of dosimeters. The study demonstrated over 30% over-response in radiographic films and less than 10% in TLDs, particularly in small field sizes and IMRT.

Concerning small field sizes, to the best of our knowledge, just a few studies have evaluated electron and photon energy spectra in water both inside and outside of the radiation field (Xicohténcatl-Hernández et al., 2021). This is a highly complex undertaking because the energy spectrum outside the field edge changes as a function of depth, distance away from the beam central axis, and field size (Kry et al., 2017; Jang et al., 2007; H. Liu and Verhaegen, 2002). To overcome this challenge, most researchers have used Monte Carlo methods (Kry et al., 2006; Skrobala et al., 2017; Scarboro et al., 2011; Edwards and Mountford, 2004). These methods have already demonstrated effectiveness and accuracy in simulating in-field doses, making them valuable for calculating out-of-field doses.

We undertook the current study to investigate the variability in the energy spectrum and mean energy of several 6 MV medical linear accelerators of Varian TrueBeam^{TM}, Varian Clinac ix^{TM}, Elekta Precise and Mohan spectrum as a function of field size and measurement location for small radiotherapy fields. This study aims to understand the secondary effects of modern radiotherapy treatments and determine the impact of spectral variations on energy-dependent dosimeters.

2 Materials and Methods

The study utilized IAEA phase space files of Varian TrueBeam^{TM} and Varian Clinac ix^{TM} linear accelerators (Varian Oncology Systems, Palo Alto, CA), as well as the Elekta Precise linear accelerator operating in a 6 MV photon beam. These files were modeled using the BEAMnrc Monte Carlo code (Kawrakow and Rogers, 2016). Researchers previously validated each linear accelerator model. The Varian TrueBeam phase space file was produced by Constantin et al. (Constantin et al., 2010) and the Varian Clinac ix file was validated by Hedin et al. (Hedin et al., 2010). The Elekta Precise model was validated by Tonkopi et al. (Tonkopi et al., 2005) and McEwen et al. (McEwen et al., 2008). The IAEA phase space files generated from the machine head were then used as inputs for a component module to simulate photon and electron spectra of a 6 MV photon beam for several field sizes (www-nds.iaea.org). Additionally, a 6 MV pre-defined spectrum by Mohan et al. (Mohan et al., 1985) was also added for comparison with the other three linacs.

The aim of this study is to calculate photon and electron fluences at points within the field, outside the field and at the edge of the radiation field sizes. The calculations were carried out for circular field sizes of 0.75 cm, 1.0 cm, 2 cm, 2.5 cm, 3 cm, 3.5 cm, 4 cm, and 5 cm, as well as for the reference field size of 10 cm. For each field size, photon energy spectra were calculated at several water depths (i.e., 0.125, 1.5, 5, and 10 cm) and off-axis distances using

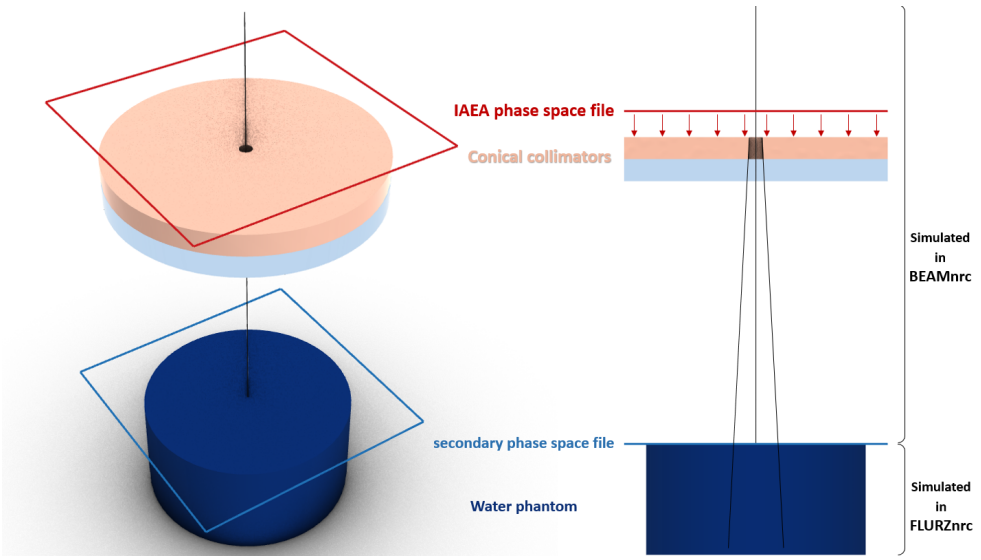

Figure 1: The geometry simulated for the Varian TrueBeam™, Elekta Precise, and Varian Clinac IX linac. for the pre-defined 6 MV spectrum, the section simulated in FLURZnrc was only used.

the FLURZnrc module of the EGSnrc code.

The water depths in this study include the Dmax (1.5 cm for a 6 MV photon beam), as well as 5 and 10 cm depths, which are commonly used as reference depths in dosimetry calculations. Furthermore, the photon and electron fluence spectra were scored within cylindrical voxels of 0.5 cm height and variable radius of 0.15 cm for 0.75 cm field size to 0.5 cm for larger ones. The simulation was conducted on a large water phantom of $50 \times 50 \times 50$ cm^3 at 100 cm source to surface distance (SSD), with photon and electron flux voxels added throughout the water phantom, including several in-field and out-of-field positions.

In all simulations, a logarithmic energy binning structure from 10 keV to 6 MeV was employed, and the electron cut-off (ECUT) and photon cut-off (PCUT) energies were defined at 0.521 MeV and 0.01 MeV, respectively. The relative error values for the photon fluence spectrum, where the relative frequency is more than 5% of the maximum frequency value, are approximately 1%. In comparison, the relative error for the electron spectrum is less than 2%. The geometry of Varian TrueBeam™, Elekta Precise™, and Varian Clinac ix™ linac as well as the pre-defined 6 MV Mohan spectrum, which are simulated by FLURZnrc code, have been presented in Fig. 1.

It should be noted that while the BEAMnrc code allows the simulation of square fields using the secondary collimators, the FLURZnrc module of the EGSnrc Monte Carlo code only allows cylindrical geometries to be converted into equivalent circular fields. Thus, to calculate the fluences, the square fields were converted into equivalent circular field sizes according to the following equation (Boles, 1972; Xicohténcatl-Hernández et al., 2021):

$$L = d\,(0.891 + 0.00046\,d) \qquad (1)$$

where L is the length of the equivalent square field size, and d is the diameter of the circular field size. The equivalent square field sizes for square fields with side lengths of 0.7, 0.9, 1.8, 2.2, 2.7, 3.1, 3.6, 4.5, and 9.0 cm correspond to circular fields with diameters of 0.75, 1.0, 2.0, 2.5, 3.0, 3.5, 4.0, 5.0, and 10.0 cm, respectively.

We decided to use conical collimators to create circular fields instead of square fields. This choice was influenced by the fact that the FLURZnrc code, which calculates particle fluence, operates in cylindrical coordinates and defines output voxels in cylindrical coordinates as well. By using circular fields, we maintain symmetry and simplicity in our calculations, allowing us to focus on studying changes in the photon and electron fluence spectrum at different off-axis distances and depths for a given field. If we were to use square fields, the complexities of the shape would unnecessarily complicate our analysis. Moreover, using square fields would expose some parts of the voxels to the corners of the field, which is not ideal for our research.

3 Results

3.1 Photon Fluence Spectra

Using Monte Carlo simulation, we calculated variations in the photon energy spectra of a 6 MV photon beam as a result of different treatment parameters, including field size and measurement location. Figure 2 presents the energy photon fluence normalized to the total fluence of the corresponding voxel for a 5 cm circular field size. The number of histories in our MC simulations is around 10^9 and subsequently the statistical uncertainties related to the flux are on the order of <1%.

The results show that changes in depth caused a more pronounced difference in the photon spectra than the distance away from the central axis for out-of-field regions, as beyond Dmax (i.e. the depth at which the dose reaches its maximum value. For a 6 MV photon beam, Dmax is approximately 1.5 cm), the photon spectra were weighted towards low-energy photons (photon energies below 100

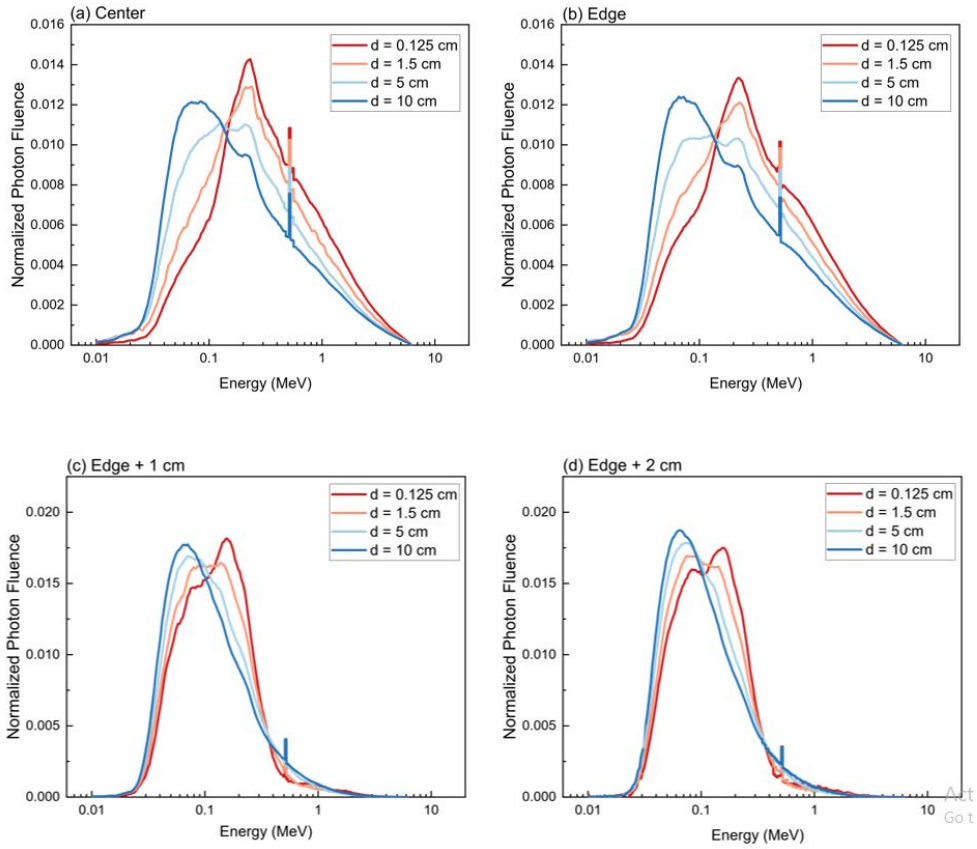

Figure 2: Normalized photon fluence as a function of photon energy at several depth and four off-axis distances for a 5 cm circular field size. a) central of axis, b) field edge, c) 1 cm from the field edge, d) 2 cm from the field edge.

keV). The reason behind this behavior is attributed to the increased number of Compton scattering as the water volume becomes larger. As seen in Fig. 2, for a given field size, as the distance away from the central axis increased, the photon energy spectra became softer.

As a result, the photon spectra were shifted significantly towards lower energy components at deeper depths, at farther distances from the field edge, and in larger fields due to the presence of scattered photons in water. To elaborate, the energy of the photon with its maximum frequency decreases from about 230 keV at the surface to about 60 to 90 keV at greater depths. Beyond the field boundaries, for example, 2 cm from the edge, the photon spectra reach a maximum frequency at a photon energy of about 160 keV at the surface. However, this energy related to the maximum frequency decreases to about 60-80 keV at depths of 1.5 cm, 5 cm, and 10 cm.

A further feature of the photon spectra (Fig. 2) is the narrow peak at 0.511 MeV due to positron annihilation, which occurred predominately in the high-energy atomic number components, independent of the water depth. Using all photon spectra, the photon mean energy was calculated for several field sizes, off-axis distances, and depths. These data are displayed in Figs. 3 and 4. Figure 3 presents the mean photon energy as a function of depth at the beam central axis and field edge for different field sizes (i.e., 0.75, 1, 2, 4, 5, and 10 cm). As seen in Fig. 3, the photon mean energy at different water depths varies with the field size and changes rapidly, starting at a depth of approximately 4 cm, especially in small field sizes.

Figure 4 presents the photon mean energy as a function of off-axis distances for circular field sizes of 0.75, 2, 5, and 10 cm and several depths. The photon mean energy decreases as the field size increases within the radiation field, and it is due to more contribution of scattered photons at larger field sizes.

3.2 Electron Fluence Spectra

The study provides normalized electron fluence spectra at three depths (0.125 cm, 1.5 cm, and 10 cm) in both the central and out-of-field regions (Fig. 5). Four different models, including three linac models and a predefined spectrum, were used in the calculations. In the central region, there is no change in the electron fluence as the depth increases. Additionally, there is good agreement among the different linac models studied. In the regions +1 cm and +2 cm from the field edge, a similar spectrum is observed at a depth of 10 cm. However, the maximum electron flux compared to the beam center decreases from about 230 keV to about 60 keV. Outside of the field, there are more high-energy electrons near the surface. When comparing the different linear accelerator models, Elekta and TrueBeam are quite similar, while Clinac ix tends to produce lower energy electrons. Considering that the Mohan spectrum produces a completely different electron spectrum in this region, it also suggests that the pre-defined spectrum may not be reliable in this

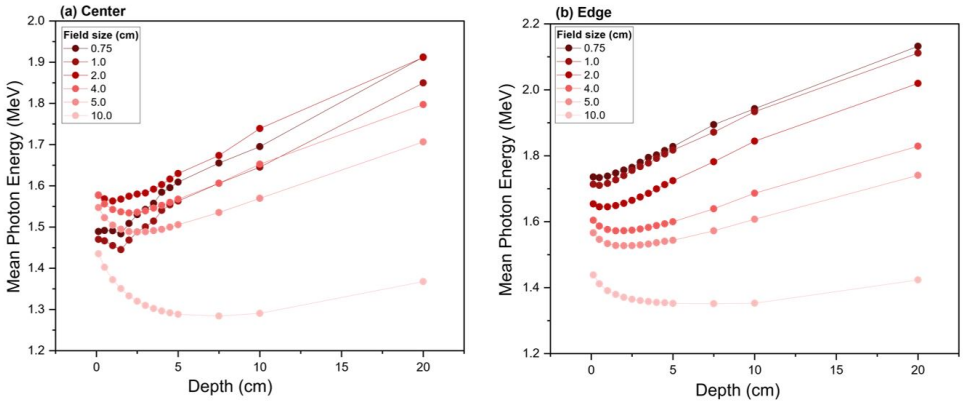

Figure 3: Mean photon energy as a function of depth for several square field sizes at a) central of axis, b) field edge.

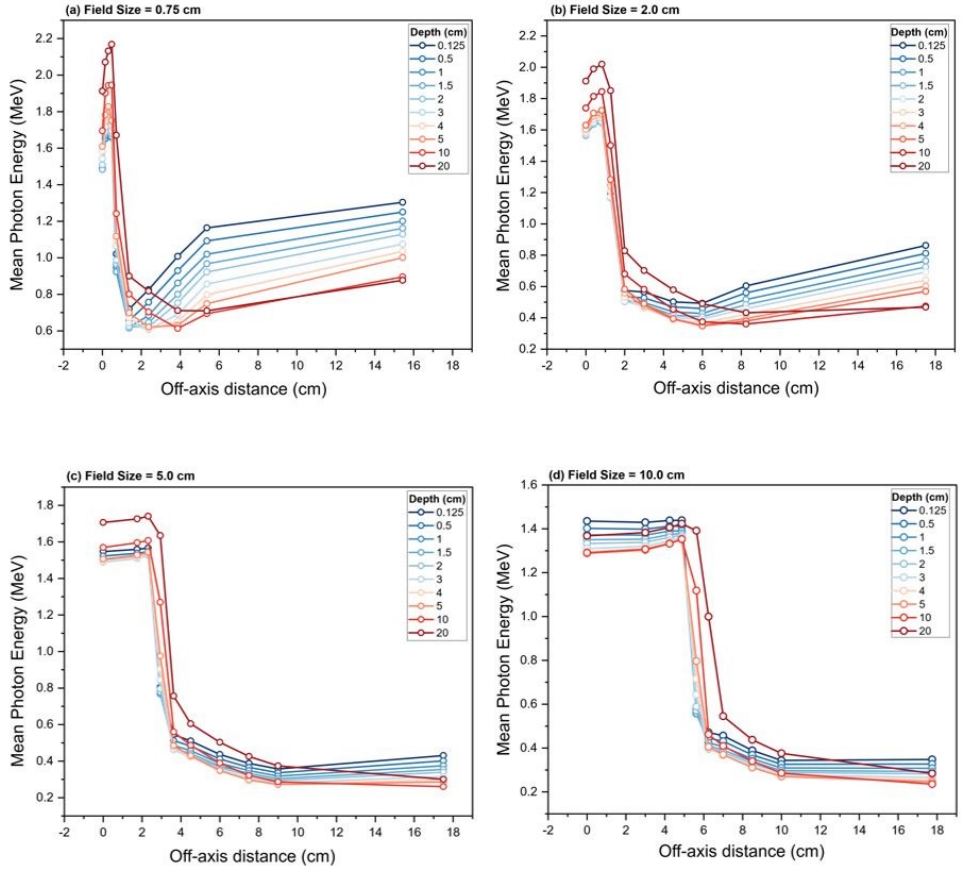

Figure 4: Mean photon energy as a function of off-axis distances for field sizes of a) 0.75 cm, b) 2 cm, c) 5 cm and d) 10 cm and several depths.

specific region.

Using all electron spectra, the mean electron energy has been calculated for several field sizes, off-axis distances and depths. These data are displayed in Figs. 6 and 7. Figure 6 presents the mean electron energy as a function of distance away from the field edge for two circular field sizes: a small field of 0.75 cm and a larger 10 cm field size. The data clearly indicates variation in the mean electron energy as a function of depth, field size and off-axis distance.

Figure 7 presents the mean electron energy as a function of depth at several field sizes for beam centeral axis and field edges. As seen in this figure, the mean electron energy at shallow depths are similar in all field sizes (0.75 MeV), but for a given field size at deeper depth, the mean electron energy increased. Also as shown in Fig. 7, as the field size increased, the mean electron energy decreased.

4 Discussion

4.1 Mean Photon Energy

Figure 3 indicates that the photon mean energy in the beam central axis and the field edge at different water

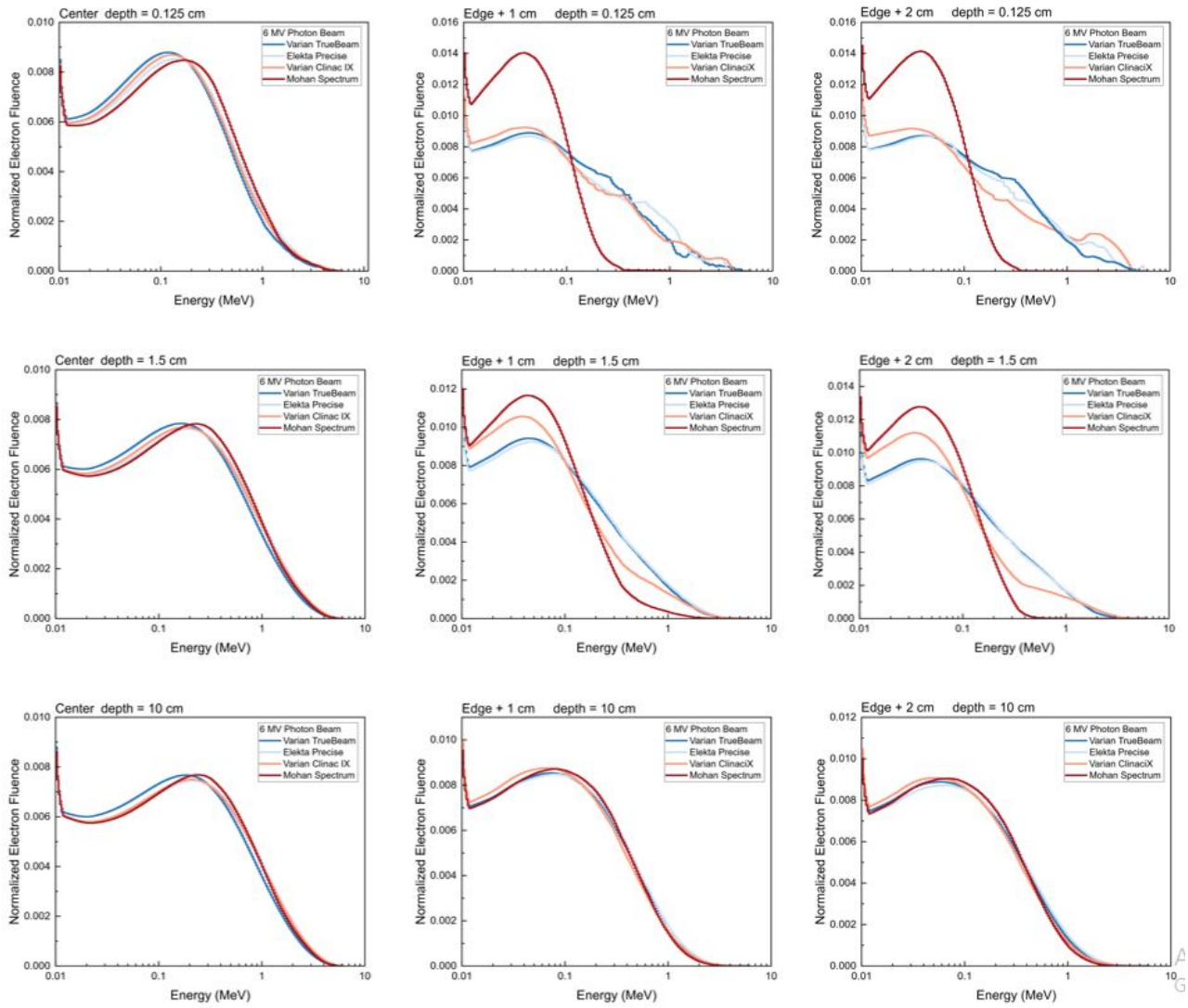

Figure 5: Normalized electron fluence as a function of photon energy at several depth and four off-axis distances for a 5 cm circular field size. a) central of axis, b) field edge, c) 1 cm from the field edge, d) 2 cm from the field edge.

depths varies with the field size. The photon mean energy along both the beam central axis and the field edge decreased with the field size as scattered low-energy photons became more dominant in larger fields. In contrast to the small fields where the photon mean energy in the beam central axis rises as the depth increases, in the 10 cm field size, the photon mean energy decreases with the water depth. That is, deeper depths lead to a larger volume of water where the primary beam interacts to produce more Compton photons, resulting in a softer photon-energy spectrum.

Also, in the beam central axis and edge of the fields, the photon mean energy close to the water surface is about 1.4 MeV for a 10 cm field size and 1.6 MeV to 1.7 MeV in smaller field sizes of 0.75, 1, 2, 4, and 5 cm. Note that in the beam central axis of small field sizes, the photon mean energy at shallow depths, i.e., 0.125 and 0.5 cm, are similar, whereas, in the 10 cm field size, the differences are more considerable. The similarity of the photon spectra at shallow depths could be due to the lack of charged particle equilibrium (CPE) in the vertical direction of the beam. However, a similar trend is observed on the edge of the fields in different field sizes.

The current findings suggest that the photons scattered within the water phantom at a given depth hold greater importance than those originating from the phantom's surface. These findings demonstrate a correlation between the mean photon energy and the field size, which can be useful in the development of radiation therapy planning techniques.

Figure 4 indicates that the photon mean energy is depth-dependent within the radiation field, where at shallow depth (i.e., 0.125 cm), the photon mean energy at all field sizes is around 1.5 MeV. However, at deeper depth (i.e., 20 cm), the photon mean energy decreases as the field size increases, where the mean photon energy varies from 1.91 MeV in 0.75 cm field size to 1.36 MeV in 10 cm field size, and it is due to more contribution of scattered photons. In the edge of the fields, the same trend is observed where the photon mean energy varies from 1.73

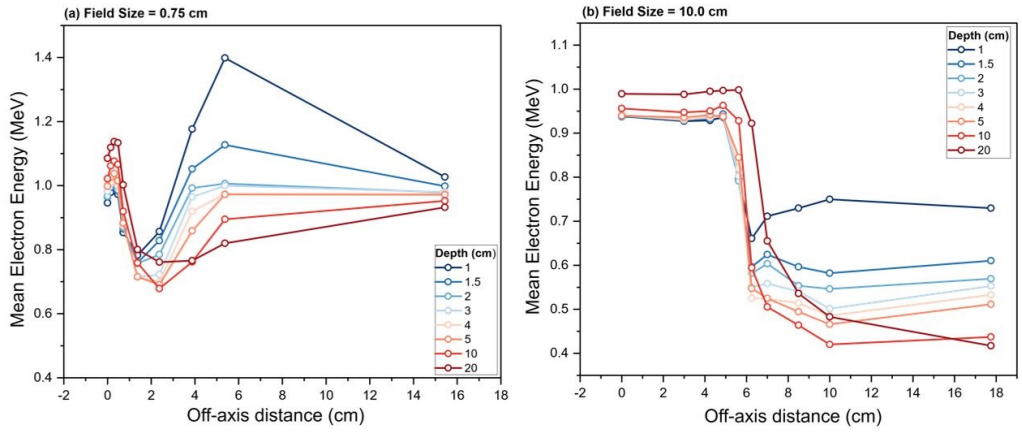

Figure 6: Mean electron energy as a function of off-axis distances and several depths for a) 0.75 cm and b) 10 cm circular field sizes.

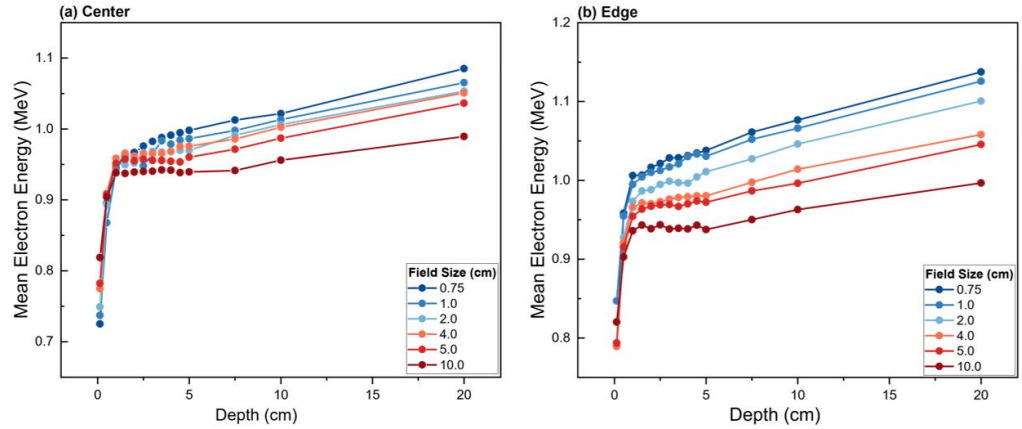

Figure 7: Mean electron energy as a function of depth for several square field sizes at a) central of axis and b) field edge.

MeV at 0.75 cm field size to 1.43 MeV at 10 cm field size in 0.125 cm water depth, and from 2.13 MeV at 0.75 cm field size to 1.42 MeV at 10 cm field size in 20 cm water depth. However, an inverse trend is observed outside the field edge, where the photon mean energy decreases as we move away from the field edge, reaches a minimum, and then increases as the off-axis increases. As seen in Fig. 4, the photon mean energy at 1 cm to 2 cm from the field edge was considerably less than in-field regions, but it increased as the distance from the field edge increased beyond 2 cm. The greater distance from the field edge allow more X-rays to undergo multiple scattering and absorption.

For out-of-field regions, for the 0.75 cm field size, at a depth of 1.5 cm and 15 cm off-axis, the photon mean energy was 1.16 MeV vs. 0.97 MeV at 5.5 cm off-axis. This trend is less pronounced in larger fields (5 cm and 10 cm); as for the 5 cm field size, at a depth of 1.5 cm and 15 cm off-axis, the mean energy level was 0.35 MeV vs. 0.30 MeV at 5.5 cm off-axis. Notably, for larger field sizes (i.e., 5 cm and 10 cm), the out-of-field photon mean energy decreases roughly exponentially with distance from the field edge.

Monte Carlo simulations showed that while the photon mean energy at dmax for a 6 MV beam is around 1.5 MV, the mean energy outside the treatment field is much lower, typically between 0.2 and 0.6 MeV; this confirms previous findings (Kry et al., 2017; Scarboro et al., 2011). Skrobala et al. (Skrobala et al., 2017) studies show that the mean energy outside of the beam decreases rapidly from 0 to 10 cm beyond the field edge at all measured depth levels. However, at distances of 15 cm and greater from the field edge, the energy levels stay within a relatively close range (0.2 to 0.25, depending on depth) and may even increase slightly.

4.2 Mean Electron Energy

Considering that electrons with low energy around 10 keV exhibit a relatively high linear energy transfer (LET), which may lead to late effects of secondary radiation on nearby healthy organs following radiotherapy treatment of a tumor, this energy range is particularly important. Therefore, it is necessary to compare different simulated models within this energy range. Figure 5 illustrates that the Clinac ix generates approximately 20% more low-energy electrons at the phantom's surface compared to the other two linacs under investigation, necessitating special attention.

Figure 6 indicates that for a given field size (i.e. 0.75 cm or 10 cm), the mean electron energy increases with

depth inside the field, while similar to photons, the mean electron energy decreases with increasing field size in the beam central axis and the edge of the fields.However, outside of the field edge, the behavior of electrons is depth-dependent. The mean electron energy beyond the field edge displays a different pattern with a minimum and a maximum value, depending on the field size and the water depth. This is due to the increase in the scattering radiation outside the field boundaries. Ultimately, at larger off-axis distances, it seems that the mean electron energy reaches a constant value, i.e., at about 10 cm from the central axis, the mean electron energy was nearly constant for a 0.75 cm field size. Xicohtncatl-Hernndez et al. (Xicohténcatl-Hernández et al., 2021) found that there is a significant difference in the total electron fluence between the 4.5 and 0.7 cm^2 field sizes at depths of 1.35 cm and 9.85 cm in the central axis, with a difference of approximately 21% and 30%, respectively. Concerning the data shown in Fig. 6, at 1 and 2 cm beyond the field edge, the mean electron energies are higher than those for photons. This could possibly be attributed to the primary electrons leaking from the linac head, causing contamination. This result is of prominent importance due to the relatively high LET of these electrons, which may have a significant impact on the healthy tissue surrounding the tumor volume despite the delivered dose being considered small. This is why it is crucial to consider these electrons from a radiation protection standpoint to protect the patient's skin during radiotherapy treatment using linear accelerators.

For energy-dependent dosimeters, it is generally assumed that the energy spectrum is constant inside the field and is unperturbed by field size, depth, and off-axis distances. Although, the dosimeter response was not significantly affected by the spectral variations (<1% effect) for most in-field measurements. However, a correction factor is generally necessary for out-of-field measurement points where the spectrum is much softer. If these variations do not count, it introduces errors in clinical dose measurement (Scarboro et al., 2011).

5 Conclusions

We examined the changes in the energy and distribution of photons and electrons for three commonly used linear accelerators and a standard 6 MV spectrum. This was done for small and standard radiation therapy fields outside of the main treatment area. Our research revealed that the energy distribution and mean energy of the beams are influenced by their spatial position and vary significantly based on depth, off-axis distance, field size, and the specific linear accelerator model. We also observed that the average photon energy decreases noticeably outside the 6 MV photon beam at all depths. Additionally, we found that the behavior of electrons is depth-dependent beyond the field edge, with higher average electron energy near the surface compared to the in-field regions, particularly for small fields. These high Linear Energy Transfer (LET) electrons should be taken into account, as they impact healthy tissues around the tumor and result in increased surface radiation dose.

Conflict of Interest

The authors declare no potential conflict of interest regarding the publication of this work.

References

Boles, M. (1972). Central axis depth dose data for use in radiotherapy.

Bordy, J. M., Bessieres, I., d'Agostino, E., et al. (2013). Radiotherapy out-of-field dosimetry: Experimental and computational results for photons in a water tank. *Radiation Measurements*, 57:29–34.

Chetty, I. J., Curran, B., Cygler, J. E., et al. (2007). Report of the AAPM Task Group No. 105: Issues associated with clinical implementation of Monte Carlo-based photon and electron external beam treatment planning. *Medical Physics*, 34(12):4818–4853.

Constantin, M., Constantin, D. E., Keall, P. J., et al. (2010). Linking computer-aided design (CAD) to Geant4-based Monte Carlo simulations for precise implementation of complex treatment head geometries. *Physics in Medicine & Biology*, 55(8):N211.

D'agostino, E., Bogaerts, R., Defraene, G., et al. (2013). Peripheral doses in radiotherapy: A comparison between IMRT, VMAT and Tomotherapy. *Radiation Measurements*, 57:62–67.

Diallo, I., Haddy, N., Adjadj, E., et al. (2009). Frequency distribution of second solid cancer locations in relation to the irradiated volume among 115 patients treated for childhood cancer. *International Journal of Radiation Oncology* Biology* Physics*, 74(3):876–883.

Edwards, C. and Mountford, P. (2004). Near surface photon energy spectra outside a 6 MV field edge. *Physics in Medicine & Biology*, 49(18):N293.

H. Liu, H. and Verhaegen, F. (2002). An investigation of energy spectrum and lineal energy variations in mega-voltage photon beams used for radiotherapy. *Radiation Protection Dosimetry*, 99(1-4):425–427.

Harrison, R. (2013). Introduction to dosimetry and risk estimation of second cancer induction following radiotherapy. *Radiation Measurements*, 57:1–8.

Hedin, E., Bäck, A., Swanpalmer, J., et al. (2010). Monte Carlo simulation of linear accelerator Varian Clinac iX. *Report MFT-Radfys*, 1.

Howell, R. M., Hertel, N. E., Wang, Z., et al. (2006). Calculation of effective dose from measurements of secondary neutron spectra and scattered photon dose from dynamic MLC IMRT for, and beam energies. *Medical Physics*, 33(2):360–368.

Howell, R. M., Scarboro, S. B., Kry, S., et al. (2010). Accuracy of out-of-field dose calculations by a commercial treatment planning system. *Physics in Medicine & Biology*, 55(23):6999.

Huang, J. Y., Followill, D. S., Wang, X. A., et al. (2013). Accuracy and sources of error of out-of field dose calculations by a commercial treatment planning system for intensity-modulated radiation therapy treatments. *Journal of Applied Clinical Medical Physics*, 14(2):186–197.

Jang, S. Y., Liu, H. H., and Mohan, R. (2008). Underestimation of low-dose radiation in treatment planning of intensity-modulated radiotherapy. *International Journal of Radiation Oncology* Biology* Physics*, 71(5):1537–1546.

Jang, S. Y., Liu, H. H., Mohan, R., et al. (2007). Variations in energy spectra and water-to-material stopping-power ratios in three-dimensional conformal and intensity-modulated photon fields. *Medical Physics*, 34(4):1388–1397.

Kase, K. R., Svensson, G. K., Wolbarst, A. B., et al. (1983). Measurements of dose from secondary radiation outside a treatment field. *International Journal of Radiation Oncology* Biology* Physics*, 9(8):1177–1183.

Kawrakow, I. and Rogers, D. (2016). The EGSnrc code system: Monte Carlo simulation of electron and photon transport NRCC PIRS-701. *Ottawa: National Research Council Canada*.

Konefał, A., Orlef, A., and Maniakowski, Z. (2010). Influence of the radiation field size and the depth in irradiated medium on energy spectra of the 6 MV X-ray beams from medical linac. *Pol J Environ Stud Ser Monogr*, 1:115–118.

Kruszyna, M., Adamczyk, S., Skrobała, A., et al. (2017). Low dose out-of-field radiotherapy, part 1: Measurement of scattered doses. *Cancer/Radiothérapie*, 21(5):345–351.

Kry, S. F., Bednarz, B., Howell, R. M., et al. (2017). AAPM TG 158: measurement and calculation of doses outside the treated volume from external-beam radiation therapy. *Medical Physics*, 44(10):e391–e429.

Kry, S. F., Salehpour, M., Followill, D. S., et al. (2005). The calculated risk of fatal secondary malignancies from intensity-modulated radiation therapy. *International Journal of Radiation Oncology* Biology* Physics*, 62(4):1195–1203.

Kry, S. F., Titt, U., Pönisch, F., et al. (2006). A Monte Carlo model for calculating out-of-field dose from a Varian beam. *Medical Physics*, 33(11):4405–4413.

McEwen, M., Kawrakow, I., and Ross, C. (2008). The effective point of measurement of ionization chambers and the build-up anomaly in MV x-ray beams. *Medical Physics*, 35(3):950–958.

Mesbahi, A., Fix, M., Allahverdi, M., et al. (2005). Monte Carlo calculation of Varian 2300C/D Linac photon beam characteristics: a comparison between MCNP4C, GEANT3 and measurements. *Applied Radiation and Isotopes*, 62(3):469–477.

Mohan, R., Chui, C., and Lidofsky, L. (1985). Energy and angular distributions of photons from medical linear accelerators. *Medical Physics*, 12(5):592–597.

Newhauser, W. D., De Gonzalez, A. B., Schulte, R., et al. (2016). A review of radiotherapy-induced late effects research after advanced technology treatments. *Frontiers in Oncology*, 6:13.

Newhauser, W. D. and Durante, M. (2011). Assessing the risk of second malignancies after modern radiotherapy. *Nature Reviews Cancer*, 11(6):438–448.

Reynaert, N., Coghe, M., De Smedt, B., et al. (2005). The importance of accurate linear accelerator head modelling for IMRT Monte Carlo calculations. *Physics in Medicine & Biology*, 50(5):831.

Sánchez-Nieto, B., Medina-Ascanio, K. N., Rodríguez-Mongua, J. L., et al. (2020). Study of out-of-field dose in photon radiotherapy: A commercial treatment planning system versus measurements and Monte Carlo simulations. *Medical Physics*, 47(9):4616–4625.

Scarboro, S. B., Followill, D. S., Howell, R. M., et al. (2011). Variations in photon energy spectra of a 6 MV beam and their impact on TLD response. *Medical Physics*, 38(5):2619–2628.

Skrobala, A., Adamczyk, S., Kruszyna-Mochalska, M., et al. (2017). Low dose out-of-field radiotherapy, part 2: Calculating the mean photon energy values for the out-of-field photon energy spectrum from scattered radiation using Monte Carlo methods. *Cancer/Radiothérapie*, 21(5):352–357.

Tonkopi, E., McEwen, M., Walters, B., et al. (2005). Influence of ion chamber response on in-air profile measurements in megavoltage photon beams. *Medical Physics*, 32(9):2918–2927.

Wang, L. and Ding, G. X. (2014). The accuracy of the out-of-field dose calculations using a model based algorithm in a commercial treatment planning system. *Physics in Medicine & Biology*, 59(13):N113.

Xicohténcatl-Hernández, N., Moreno-Ramirez, A., and Massillon-JL, G. (2021). Electron and photon energy spectra outside of 6 MV X-ray small radiotherapy field edges produced by a Varian iX Linac. *Frontiers in Physics*, 9:656922.

To cite this article:

Khodabandeh Baygi, V., Rafat-Motavalli, L., Hoseinian-Azghadi, E. (2025). Determination of photon and electron fluence spectral variation for 6 MV medical linear accelerators by Monte Carlo simulation. Radiation Physics and Engineering, 6(1), 21-29. doi: 10.22034/rpe.2024.465869.1200

DOI: 10.22034/rpe.2024.465869.1200

To link to this article: https://doi.org/10.22034/rpe.2024.465869.1200